The Dark Stable Tyrosine Radical of Photosystem 2 Studied in Three Species Using ENDOR and EPR Spectroscopies[†]

Stephen E. J. Rigby,[‡] Jonathan H. A. Nugent,[*,‡] and Patrick J. O'Malley[§]

Department of Biology, Darwin Building, University College London, Gower Street, London WC1E 6BT, U.K., and Department of Chemistry, UMIST, P.O. Box 88, Manchester M60 1QD, U.K.

Received May 20, 1993; Revised Manuscript Received October 13, 1993[®]

ABSTRACT: The dark stable neutral tyrosine radical $Y_D^{\bullet}$ of photosystem 2 (PS2) has been studied using electron nuclear double-resonance (ENDOR) and electron paramagnetic resonance (EPR) spectroscopies. The proton hyperfine coupling constants of all four ring protons and both β-methylene protons have been determined for $Y_D^{\bullet}$ in three species covering the range of oxygenic organisms; a higher plant (spinach), an alga (*Chlamydomonas reinhardtii*), and a cyanobacterium (*Phormidium laminosum*). It has generally been assumed that the properties of $Y_D^{\bullet}$ are the same in all oxygenic organisms, while in fact there are small but significant differences. The β-proton coupling constants are shown to be species dependent while the ring proton coupling constants are not. Estimation of the electron spin density distribution of $Y_D^{\bullet}$ from all three organisms has been done. This shows that changes in β-proton coupling constants in each organism arise from the slightly different orientation of the tyrosine ring, relative to the β-protons. The electron spin density distribution within the tyrosine ring is organism independent. The variations in the β-proton coupling constants are reflected in the corresponding EPR spectra, where small variations in line width have been detected. These data delineate the range of natural variation in the spectroscopic properties of $Y_D^{\bullet}$, and by assigning the features of the ENDOR spectrum, provide a basis for both the unification of studies of $Y_D^{\bullet}$ in different organisms and the study of $Y_Z^{\bullet}$. The results are discussed in relation to data in the recent study (Hoganson & Babcock, 1992) using $Y_D^{\bullet}$ in the cyanobacterium, *Synechocystis* PCC 6803.

Oxidation of tyrosine in aqueous solution at neutral pH releases the phenoxyl proton to produce the tyrosine neutral radical (Figure 1) (DeFilippis et al., 1989, 1991). The E_m of the neutral radical is one of the lowest among those of the 20 common amino acids at 0.93 V vs NHE (DeFilippis et al., 1989, 1991; Harriman, 1987). Therefore neutral tyrosine radicals may be formed in proteins with relatively long lifetimes as they will not easily oxidize their protein environments. For this reason neutral tyrosine radicals are ideal constituents of high potential biological redox systems. Such radicals have been identified in ribonucleotide reductase (Sjöberg & Gräslund, 1983; Bender et al., 1989), PS2[1] (Barry & Babcock, 1987), and prostaglandin H synthase (Smith et al., 1992; DeGray et al., 1992). Covalently modified analogues have been identified in *Dactylium dendroides* galactose oxidase (*o*-cysteine substituted) (Whittaker & Whittaker, 1990; Babcock et al., 1992) and amine oxidases (6-hydroxytopaquinone) (Janes et al., 1990).

Tyrosine radicals in PS2 are generated by the action of the oxidizing species $P680^+$, the photogenerated cation of the primary donor. Two such tyrosine radicals have been identified by using site directed mutagenesis in cyanobacteria (Debus et al., 1988a,b; Vermaas et al., 1988; Metz et al., 1989). One of these, $Y_Z^{\bullet}$, constitutes the link between P680 and the oxygen-evolving complex (OEC), by which it is rereduced (Babcock & Sauer, 1973; Babcock et al., 1989). The other, $Y_D^{\bullet}$, is stable in the oxidized state for hours but is able to slowly undergo redox reactions with the lower oxidation states of the OEC in the dark (Styring & Rutherford, 1987; Nugent et al., 1987). The slower rate of oxidation of Y_D by $P680^+$ also suggests that, unlike Y_Z, it is not involved in the main electron transfer pathway in PS2. The function of Y_D may be linked to the properties of neutral tyrosine radicals mentioned above, i.e., it may represent a way in which "stray" oxidizing equivalents can be stored with minimal damage to the protein. Y_Z has been identified as Tyr161 of the D1 protein (psbA gene product) and Y_D as Tyr161 of the D2 protein (psbD gene product) (Debus et al., 1988a,b; Vermaas et al., 1988; Metz et al., 1989). The D1 and D2 proteins are throught to form a 1:1 complex with *C*2 symmetry analogous to the LM complex of the bacterial reaction center (Svensson et al., 1990; Ruffle et al., 1992). Therefore Y_Z and Y_D are expected to be symmetrically placed about P680, and the differences in the observed oxidation rates must arise from factors such as

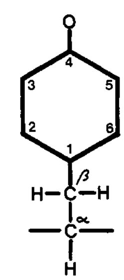

FIGURE 1: Numbering scheme for the carbon atoms of the tyrosine neutral radical.

[†] We acknowledge financial assistance from the U.K. Science and Engineering Research Council.

[*] Address correspondence to this author.
[‡] University College London.
[§] UMIST.

[®] Abstract published in *Advance ACS Abstracts*, February 1, 1994.

[1] Abbreviations: Chl, chlorophyll; EPR, electron paramagnetic resonance spectroscopy; ENDOR, electron nuclear double-resonance spectroscopy; HEPES, 4-(2-hydroxyethyl)-1-piperazineethanesulfonic acid; Hpp, peak to trough linewidth of EPR spectrum; MES, 2-(*N*-morpholino)-ethanesulfonic acid; OEC, the manganese-containing oxygen-evolving complex of PS2; PS2, photosystem 2; P680, the primary donor chlorophyll-(s) of PS2; $Y_D^{\bullet}$, the dark stable tyrosine (D2 161) radical of PS2; Y_Z, the tyrosine residue (D1 161) between the OEC and P680.

0006-2960/94/0433-1734$04.50/0

the orientations or environments of the tyrosine residues and the proximity of the manganese complex of the OEC.

Since tyrosine radicals are paramagnetic, they can be studied using EPR and ENDOR spectroscopies. Indeed tyrosine radicals provided the first EPR spectra to be associated with PS2 (Commoner et al., 1956). The spectra are anisotropically broadened, with small g anisotropy and partially resolved hyperfine structure. The EPR spectrum of $Y_D^•$ is observable in the dark, while the spectrum of $Y_Z^•$ is only observable after short light flashes (Blankenship et al., 1975) or in the light and in the presence of inhibitors that prevent rapid rereduction of $Y_Z^•$ by the OEC (Babcock & Sauer, 1973). The EPR spectra of $Y_Z^•$ and $Y_D^•$ appear to be very similar (Barry & Babcock, 1987), and therefore a thorough understanding of the spectroscopic properties of $Y_D^•$ is also a good starting point in the study of $Y_Z^•$. Presumably because of the deprotonation associated with the formation of the neutral radical, $Y_Z^•$ is not observable below 230 K (Babcock & Sauer, 1973; Ono & Inoue, 1989). $Y_D^•$, once formed, may be trapped for studies at cryogenic temperatures. Such low temperatures are necessary for ENDOR studies of this system. ENDOR enables hyperfine coupling constants to be measured far more accurately than EPR, and also allows for the detection of small hyperfine couplings to which the EPR spectrum is largely insensitive.

The EPR spectra of $Y_D^•$ in several organisms are similar, and for this reason data from different organisms have been used interchangeably. However, no comparative study of $Y_D^•$ in different organisms has been attempted. A recent study (Hoganson & Babcock, 1992) presented extensive analysis of the $Y_D^•$ EPR spectrum from *Synechocystis* PCC 6803 through simulation of spectra from oriented and selectively deuterated preparations. This analysis supports the assertion that EPR spectra of tyrosine neutral radicals are dominated by one nearly isotropic β-proton hyperfine coupling and coupling to two very nearly equivalent ring protons with larger anisotropy (Fasanella & Gordy, 1969; Bender et al., 1989). Partial ENDOR spectra from spinach and *Synechocystis* PCC 6803 showing resonances arising from the large β-proton coupling were also presented, but differences between the two were attributed to artefacts and their EPR spectra were assumed to be identical. Here we describe our recent studies of $Y_D^•$ using ENDOR and EPR spectroscopies. Combining data from higher plant (spinach), algal (*Chlamydomonas reinhardtii*), and cyanobacterial (*Phormidium laminosum*) sources, we have developed a model for the electron spin density distribution in $Y_D^•$ This model enables us to evaluate the causes of differences in the EPR and ENDOR spectra of $Y_D^•$ from different organisms and lays the foundation on which studies of mutationally or chemically altered tyrosine environments in PS2 may be combined.

MATERIALS AND METHODS

Chloroplast thylakoid membranes (12 mg of Chl/mL) and PS2 membranes (BBYs; Berthold et al., 1981; Chl a/Chl b ratio 2.05–2.20:1) were prepared from market spinach (*Spinacea oleracea*) by the method of Ford and Evans (1983). Thylakoid membranes and BBYs were suspended in 20 mM MES, 15 mM NaCl, 5 mM $MgCl_2$, and 100 μM EGTA, pH 6.3, containing either 20% w/v glycerol or 0.3 M sucrose.

BBYs were depleted of calcium according to a modified method of Boussac et al. (1989) as given in Hallahan et al. (1992). These EGTA/salt-washed PS2 membranes will be referred to as calcium-depleted although the extent of calcium depletion is unknown (see Debus (1992) for discussion). The calcium-depleted PS2 membranes were then collected by centrifugation or further dialyzed against 0.3 M sucrose, 20 mM MES for 3 h in the dark, in order to reconstitute the 17- and 23-kDa extrinsic polypeptides. The membranes were centrifuged at 40000g for 30 min and resuspended in 0.3 M sucrose, 20 mM MES, 10 mM NaCl, and 100 μM EGTA, pH 6.5. Buffers containing MES and sucrose were treated with Chelex prior to the addition of NaCl and EGTA to remove any calcium impurities. The membranes obtained from the calcium-depletion treatment were depleted of greater than 90% of their oxygen-evolving activity. This was measured in a Clark-type oxygen electrode at 298 K using ferricyanide and PPBQ as electron acceptors. The control was depleted membranes to which 20 mM calcium chloride was added and then incubated for 30 min on ice.

PS2 from the cyanobacterium *Phormidium laminosum* (1 mg of Chl/mL) was prepared as in Nugent et al. (1988) and Corrie et al. (1991). It was resuspended in 10 mM HEPES, 10 mM $MgCl_2$, 5 mM disodium hydrogen phosphate, and 25% v/v glycerol, pH 7.5.

Thylakoid membranes from the alga *Chlamydomonas reinhardtii* were prepared from washed cells. The cells at a concentration of 1 mg of Chl/mL were passed twice through a french press at 4000 lb/in.^{2}. Membranes were pelleted by centrifugation at 40000g for 30 min. The soft pellet was resuspended in 2.2 M sucrose, 10 mM EDTA, 5 mM HEPES, pH 7.5, giving a final concentration of 1.75 M sucrose. This was placed in centrifuge tubes and overlayered with 0.5 M sucrose, 5 mM HEPES, pH 7.5. This was centrifuged for 2 h at 100000g and 277 K, the purified membranes being collected as a band at the interface between the two layers. The membranes were washed and resuspended in 0.35 M sucrose, 5 mM $MgCl_2$, and 20 mM HEPES, pH 7.5, at 10 mg of Chl/mL.

ENDOR and EPR Spectrometry. ENDOR and EPR spectra were obtained at X-band using a Bruker ESP 300 EPR spectrometer in conjunction with a Bruker EN 003 ENDOR interface, Wavetek 3000–446 radio frequency (rf) synthesizer, EN 370 power amplifier, and EN 801 ENDOR cavity (estimated Q of 800). The Wavetek synthesizer also provided for frequency modulation of the radio frequency output. All spectra were obtained at 10 K (helium flow) using an Oxford Instruments continuous flow ESR 900 cryostat with an ITC 4 temperature controller. The impedance of the radio frequency circuit was 50 Ω. ENDOR spectra were acquired at field values corresponding to the crossing point of the first derivative EPR spectrum and were corrected for baseline nonlinearity by the substraction of off-resonance scans which were filtered for noise (standard Bruker software) to avoid reducing the spectrum signal to noise ratio. ENDOR spectra begin at 9 MHz. The only resonances below this frequency should be the low-frequency β-methylene resonances, which come outside the range of our rf synthesizer, and the 3,5 proton A_z and A_x, which are too weak to be detected. First-derivative X-band EPR spectra were recorded using the same cavity/cryostat combination. Characteristic line shapes were established by examining several sets of samples involving different PS2 preparations. A field modulation frequency of 12.5 kHz and modulation amplitude of 1.4 G were employed.

S-band EPR spectra were obtained using a Bruker Flexline S-band resonator and microwave bridge in conjunction with the above spectrometer. The temperature was maintained at 10 K using an Oxford Instruments CF935 liquid helium immersion cryostat and the above-mentioned ITC4 temperature controller. The microwave power was 10 μW, the

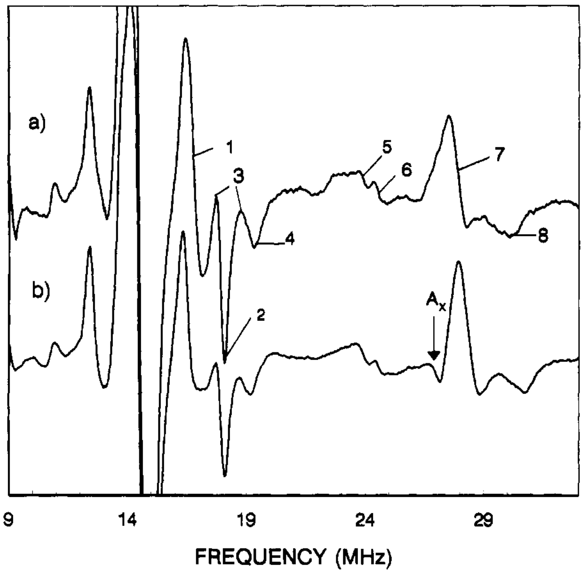

FIGURE 2: ENDOR spectra of $Y_D^\bullet$ in (a) spinach BBY membranes and (b) calcium-depleted spinach BBY membranes. Both spectra were recorded with 10 mW of microwave power, 100 W of rf power, and 158-kHz rf modulation depth. Spectra are the averages of 160 scans. Numbers and arrows refer to features of Table 1 and are also discussed in the text.

modulation frequency 100 kHz, and the modulation amplitude 1.4 G. Four scans were coadded to produce the final spectrum.

RESULTS

Higher Plant PS2. The ^{1}H ENDOR spectra of $Y_D^\bullet$ in spinach (*S. oleracea*) BBY membranes and calcium-depleted BBYs are shown in Figure 2. Lower resolution ENDOR spectra for $Y_D^\bullet$ in spinach were reported some time ago (O'Malley et al., 1984; Chandrashekar et al., 1986), but no assignments of hyperfine couplings based on a tyrosine radical origin were made. The first-derivative presentation enables us to detect turning points for the ring and β-methylene proton resonances as originally described for quinones (O'Malley & Babcock, 1984, 1986). These spectra, recorded with 158-kHz FM rf modulation depth, reveal eight resolved hyperfine couplings, Table 1. (Spectra obtained using thylakoid membranes exhibit the same hyperfine couplings as the BBY samples, not shown, but because of the dilution of PS2 these spectra have inherently lower signal to noise.) While the hyperfine coupling constants for the two types of sample are broadly similar, differences are observed for features 1, 4, 7, and 8. Previous studies of tyrosine neutral radicals in L-tyrosine hydrochloride crystals (Fasanella & Gordy, 1969; Box et al., 1974) and frozen solutions of *Escherichia coli* ribonucleotide reductase (RR) (Bender et al., 1989) have shown the hyperfine tensors for the protons on rings carbons 3 and 5 to be rhombic with A_y = 7–8.7 MHz, A_z = 18–20 MHz, and A_x = 25–27 MHz. The crystal data shows that the hyperfine couplings to protons 3 and 5 are inequivalent (Box et al., 1974), despite both being *ortho* to the phenolic oxygen. This is supported by the temperature dependence of the solution state spectrum of tyrosine hydrochloride (Van den Hoek et al., 1970). Thus the A_z feature of the 3.5 protons would be expected to arise at a frequency corresponding to a hyperfine coupling of 18–20 MHz and to be resolved into two components. These criteria are met by features 5 and 6 of Figure 2, which we therefore assign to the inequivalent A_z components of the 3,5 proton tensor. Through a similar argument we assign the broad feature 3 (Figure 2) as the A_y

Table 1: Assignments of ENDOR Spectrum Features to $Y_D^\bullet$ Protons

	feature	hyperfine coupling constant[a] (MHz)	assignment
spinach (*S. oleracea*)	1	4.4	2 or 6 A_x
		4.6	$\beta A_\perp$
		4.8	2 or 6 A_x
	2	7.15	2 or 6 A_y
		7.4	2 or 6 A_y
	3	−8.0	3 + 5 A_y
	4	9.75	$\beta A_\parallel$
	5	−19.1	3 or 5 A_z
	6	−20.5	3 or 5 A_z
	7	27.2	$\beta A_\perp$
	8	31.5	$\beta A_\parallel$
	unmarked	−25.6	3 or 5 A_x
	unmarked	−27.5	3 or 5 A_x
C. reinhardtii	1	3.9	$\beta A_\perp$
		4.4	2 or 6 A_x
		4.8	2 or 6 A_x
	2	7.15	2 or 6 A_y
		7.4	2 or 6 A_y
	3	−8.0	3 + 5 A_y
	4	9.3	$\beta A_\parallel$
	5	−19.1	3 or 5 A_z
	6	−20.5	3 or 5 A_z
	7	28.5	$\beta A_\perp$
	8	33.0	$\beta A_\parallel$
	unmarked	−25.6	3 or 5 A_x
	unmarked	−27.5	3 or 5 A_x
P. laminosum	1	4.4	2 + 6 A_x
		6.4	$\beta A_\perp$
	2	7.3	2 + 6 A_y
	3	−8.0	3 + 5 A_y
	4	11.5	$\beta A_\parallel$
	5	−19.1	3 or 5 A_z
	6	−20.5	3 or 5 A_z
	7	24.5	$\beta A_\perp$
	8	29.0	$\beta A_\parallel$
	unmarked	−25.6	3 or 5 A_x
	unmarked	−27.5	3 or 5 A_x

[a] Estimated error of measurement is ±0.05 MHz.

component of the rhombic 3,5 proton hyperfine tensor (Fasanella & Gordy, 1969; Box et al., 1974; Bender et al., 1989). The intrusion of feature 2 into this region precludes the resolution of the individual 3 and 5 proton tensors here. Solution-state EPR studies of tyrosine neutral radicals show that the isotropic hyperfine coupling constants of the protons at ring positions 2 and 6 are about 5 MHz (Sealy et al., 1985). Thus the resonances arising from the 2,6 protons would be expected at around A_{iso} = 5 MHz and to be rhombic by analogy with the 3,5 proton tensors. Features 1 and 2 of Figure 2 fulfill these criteria and are therefore assigned as the the A_x and A_y components, respectively, of the 2,6 proton couplings. This assignment is consistent with the ENDOR study of the neutral tyrosine radical in *E. coli* ribonucleotide reductase (Bender et al., 1989). The A_z component of the 2,6 proton rhombic system lays under the intense matrix region and so cannot be determined. Since the line shape of 1 is changed on calcium depletion, this resonance is probably a composite of at least two components. This assertion is investigated below.

Resonances 7 and 8 (Figure 2) move in concert on calcium depletion and form an axial system. Protons β to a π delocalized system receive unpaired electron spin density principally via hyperconjugation from the ring carbon to which the methylene group is attached (Fessenden & Schuler, 1963). Therefore the hyperfine interaction may be dominated by isotropic (contact) term, with the dipolar term being small (10–20% of isotropic) by comparison. Considering the size of the axial distortion and that all the ring protons are

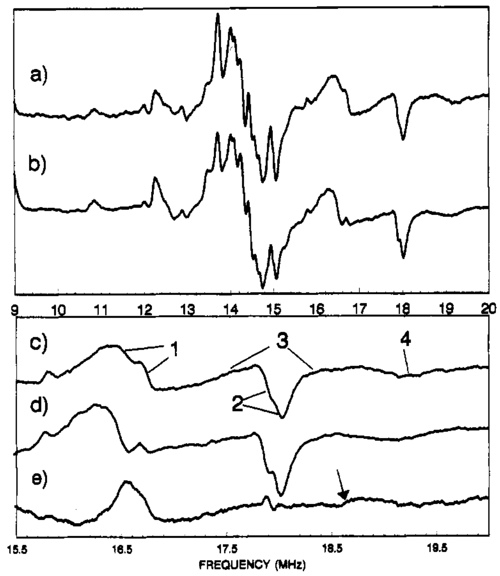

FIGURE 3: High-resolution ENDOR spectra of $Y_D^{\bullet}$ in (a and c) spinach BBY membranes, (b and d) calcium-depleted spinach BBY membranes. (e) Difference spectrum: c minus d. All spectra were recorded with 10 mW of microwave power, 63 W of rf power, and 28-kHz rf modulation depth. Spectra are the averages of 200 scans. Numbers and arrows refer to features of Table 1 and are also discussed in the text.

accounted for, we assign these features to the $A_{\perp}$ and $A_{\parallel}$, respectively, of a β-methylene proton. This leaves only feature 4 to be accounted for. The hyperfine coupling constants of both β-protons should be accompanied by changes in the coupling of the other. Comparing the spectra in Figure 2 it can be seen that as the features 7 and 8 move to higher frequency on calcium depletion, feature 4 moves to lower frequency. Therefore feature 4 and perhaps the change in feature 1 may be associated with the second β-proton. This was investigated by obtaining ENDOR spectra under high-resolution conditions.

Figure 3 shows spectra of $Y_D^{\bullet}$ obtained with 28-kHz FM rf modulation depth. This allows for much higher resolution, but at the expense of the signal to noise ratio. Under these conditions features 1 and 2 are reproducably split into two components (Figure 3c,d). This indicates that, as with the 3 and 5 ring positions, the electron spin density at the 2 and 6 ring positions is not equivalent. Such inequivalence follows from the behavior of the coupling to the 3 and 5 position protons, but it has not been observed experimentally before. The line shape of feature 1 changes on calcium depletion. The difference spectrum, Figure 3e, shows that this arises due to the movement of a third resonance superimposed on the 2,6 proton features. This resonance moves to low frequency as the β-proton resonances 7 and 8 move to high frequency. Therefore following the reasoning above, we assign this resonance as $A_{\perp}$ of the second β-proton. Feature 4 we can now assign as the $A_{\parallel}$ of the second β-proton. Note that Figure 3e also shows a feature arising from the shift of feature 4 (arrowed Figure 3e). The two β-protons of a radical methylene group are similarly, though not identically, disposed relative to the centers of electron spin density in the radical. Therefore they may be expected to have similar (though not identical) axial distortions in their ENDOR resonances. Such behavior is evident in the resonances that we assign to the tyrosine β-methylene protons.

The remaining features in the spectra of Figure 3 arise from small hyperfine couplings to protons of the protein, the tyrosine α-proton (A_{iso} in solution = *circa* 1 MHz) (Tomkiewicz et al., 1972; Sealy et al., 1985) and the A_z components of the 2,6 protons rhombic system. These small couplings are difficult to assign without the use of specific deuteration.

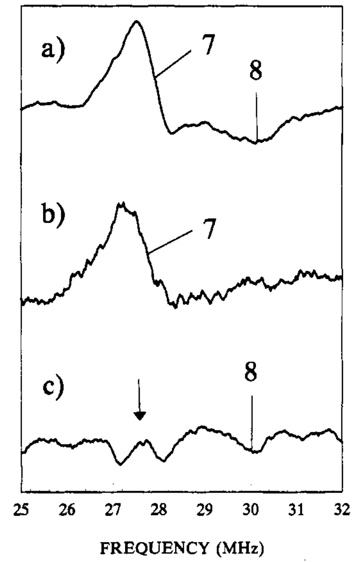

FIGURE 4: ENDOR spectra of $Y_D^{\bullet}$ in spinach BBY membranes with the field setting (a) at the EPR crossing point, (b) at g_z = crossing point plus 15 G, and (c) at g_x = crossing point minus 15 G. Numbers and arrows refer to features of Table 1 and are also discussed in the text. The signals in b and c are at the outer edge of the spectrum and are therefore weaker giving reduced signal/noise in the spectra. Other details as in Figure 2.

The A_x features of the 3,5 proton rhombic system remain to be located. The approximate value of 3,5 A_x quoted earlier would place this resonance under feature 7 (Figure 2), the β-methylene proton $A_{\perp}$. These resonances may be separated using orientation selection. The EPR powder spectrum is the sum of spectra arising from electron spins at all possible orientations to the magnetic field. Where the **g** tensor is anisotropic, however, the edges of the EPR spectrum (i.e., at field values corresponding to g_z or g_x) arise from electron spins for which the **g** tensor is oriented along the z or x axes. Therefore by acquiring ENDOR spectra at field values corresponding to the edges of the EPR spectrum, specific orientations of molecules in the **g** tensor coordinate frame may be studied. ENDOR of such specifically oriented molecules no longer produces a powder spectrum, but rather the specific components of the ENDOR spectrum arising from the orientation selected (Rist & Hyde, 1968; O'Malley & Babcock, 1986). ENDOR spectra taken at the high field edge (g_z) of the EPR spectrum will show the z components of the rhombic ring proton tensors and the $A_{\perp}$ of the β-methylene protons, and ENDOR spectra taken at the low field (g_x) edge of the EPR spectrum will show the x components of the ring proton couplings and $A_{\parallel}$ of the β-proton couplings. Note that the z principal axes of the **g** and hyperfine tensors are colinear, and the x axes diverge by only 22° (Fasanella & Gordy, 1969; Hoganson & Babcock, 1992). Spectra taken at g_z, Figure 4b, show feature 7, the β proton $A_{\perp}$, and no feature 8. Spectra taken at g_x, Figure 4c, show the $A_{\parallel}$ component (feature 8) of the β-proton coupling and a new feature at 27.6 MHz (arrowed in Figure 4c) corresponding to a hyperfine coupling of 26.6 MHz. This feature is split in two giving two A_x components of 25.6 and 27.5 MHz in keeping with the inequivalence of the protons at positions 3 and 5. Therefore, we assign this new feature as the superimposed A_x components of the 3,5 protons hyperfine couplings. Thus all the hyperfine couplings expected for a tyrosine neutral radical and all the spectrum features have been accounted for.

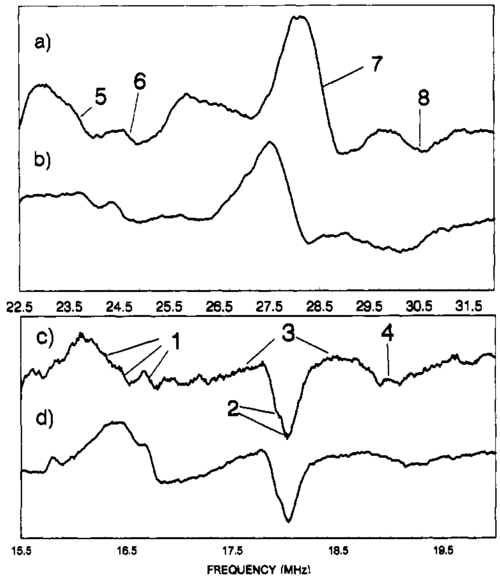

FIGURE 5: ENDOR spectra of $Y_D^•$ in *Chlamydomonas reinhardtii* thylakoid membranes, (a and c) with spectra of $Y_D^•$ in spinach BBY membranes, (b and d) for comparison. Conditions a and b as in Figure 2, c and d as Figure 3. Numbers refer to features of Table 1.

Chlamydomonas reinhardtii PS2. Although the amino acid sequences of the D1 and D2 proteins are largely conserved between photosynthetic organisms, some sequence divergence is apparent (Svensson et al., 1990; Ruffle et al., 1992). It is therefore of interest to compare the properties of higher plant $Y_D^•$ with that of the unicellular alga *C. reinhardtii.* Amino acid sequence analysis suggests that the algae diverged from the higher plants at an early stage (see Figure 1 in Ruffle et al., 1992) and that therefore *C. reinhardtii* and the higher plants studied above may represent extremes in eukaryote PS2 structure. *C. reinhardtii* also has the advantage that methods exist for the directed mutation of the photosynthetic apparatus in this organism, a procedure that is not practical for higher plants.

The EPR spectrum of $Y_D^•$ in *C. reinhardtii* membranes is 0.6 G wider than that of higher plants (see below). This should be reflected in the hyperfine coupling constants measured by ENDOR (Table 1). The ENDOR spectra are shown in Figure 5. The resonances corresponding to the large β-proton coupling (7,8) move to higher frequency compared to the higher plant spectrum (Figure 5a,b), while the smaller β-proton coupling (1,4) is resolved in the high-resolution spectrum (Figure 5c,d) and moves in the opposite sense. The hyperfine couplings to the 3,5 and the 2,6 position protons are conserved. The smaller couplings are also conserved, Table 1. These observations are consistent with the increase in the EPR line width and suggest a highly conserved environment for Y_D in eukaryotes.

Cyanobacterial PS2. Cyanobacteria represent a further stage of D1/D2 sequence divergence (Ruffle et al., 1992), particularly with regard to D2 residue 186 which is a phenylalanine in higher plants and *C. reinhardtii* but a leucine in cyanobacteria. Residue 186 is predicted to be in close proximity to Y_D (Svensson et al., 1990; Ruffle et al., 1992). We have studied $Y_D^•$ in *Phormidium laminosum* using EPR and ENDOR. The EPR spectrum of $Y_D^•$ in cyanobacteria has a line width of only 18.6 G (0.8 G narrower than higher plant $Y_D^•$, see below). This is reflected in the concomitant reduction of the large β-proton coupling (feature 7) constant observed in the ENDOR spectrum, Figure 6 and Table 1. The A_y and A_z features of the rhombic 3,5 proton coupling (features

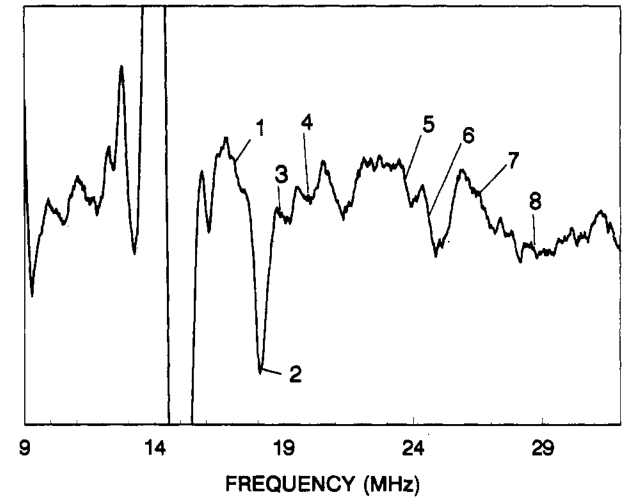

FIGURE 6: ENDOR spectrum of $Y_D^•$ in *Phormidium laminosum* PS2. Conditions as Figure 2. Numbers refer to features of Table 1.

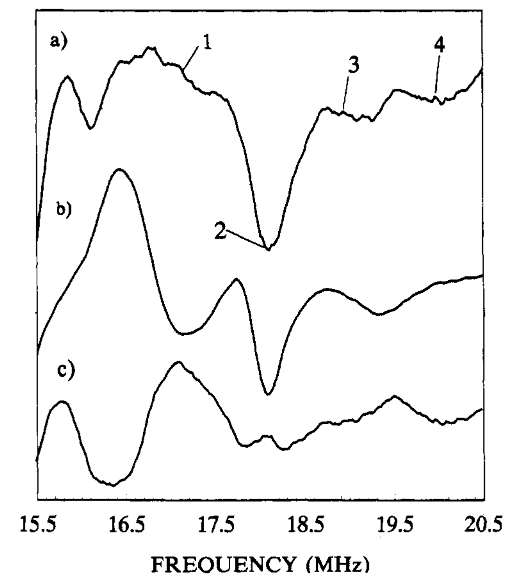

FIGURE 7: ENDOR spectra showing the smaller couplings of $Y_D^•$ in *Phormidium laminosum* (a) and spinach BBY membranes (b) for comparison. (c) Difference spectrum: a minus b. Conditions as in Figure 2.

3, 5, and 6) are identical to those of higher plants and *C. reinhardtii*, as is the inequivalence of the 3,5 proton couplings, Table 1. The broad trough between 28 and 31 MHz (feature 8) we assign to the overlapped 3,5 proton A_x feature and the $A_\parallel$ of the β-proton axial system. Some of the smaller couplings, with resonances in the region between 16 and 21 MHz, seem to be absent in cyanobacteria, Figure 7a. However, this can be rationalized by assuming that, as in eukaryotes, features in this part of the spectrum arise from the overlap of the 2,6 proton coupling with that of the second β-proton. The A_y of the 2,6 proton is clearly evident at 18 MHz, as in eukaryotes (feature 2). This suggests that the A_x component of the 2,6 proton system should also be conserved. The difference spectrum Figure 7c shows no features attributable to the 2,6 proton system, but rather the absence of the small β coupling of higher plants (negative feature in Figure 7c) and a new axial system with $A_\perp$ of 6.40 MHz and $A_\parallel$ of 11.46 MHz. This new system we assign as the smaller β-proton coupling in *P. laminosum*. Consistent with the eukaryote data, as the large β-coupling has decreased, the smaller one has increased.

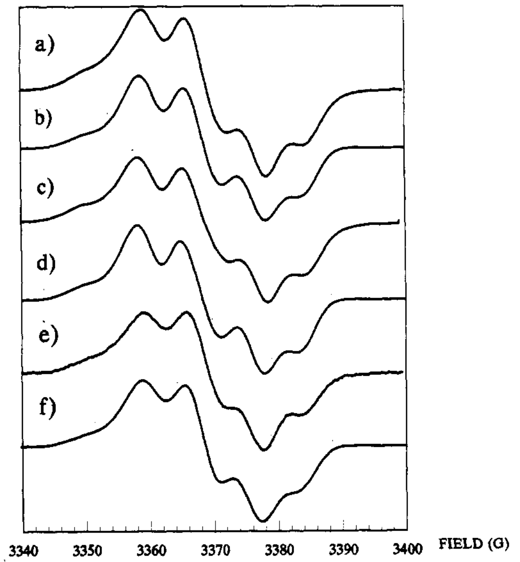

FIGURE 8: EPR spectra (a, c, and e) and simulations (b, d, and f) of $Y_D^•$ in spinach BBY membranes (a, b), *Chlamydomonas* membranes (c, d), and *Phormidium laminosum* PS2, (e, f). Spectra were recorded with 30 μW of microwave power (in the ENDOR cavity) and are the averages of four scans. Simulations were from values in Table 1 and using g values as given in Gulin et al. (1992): $g_z = 2.002\ 12$, $g_y = 2.004\ 26$, $g_x = 2.007\ 52$. Euler angles of ±22° for the 3,5 protons and ±10° for the 2,6 protons were used.

The lack of features corresponding to the 2,6 proton system in the difference spectrum, together with the 3,5 proton hyperfine coupling, suggests that we are justified in assuming that the 2,6 proton coupling is identical in cyanobacteria to that observed in higher plants and *C. reinhardtii*. The form of the spectrum (Figure 6) can thus be rationalized, taking feature 4 as the β-proton $A_{\|}$, feature 2 as the 2,6 proton A_y, and feature 1 as the overlap between the β-proton and 2,6 proton A_x. The positive part of the β-proton first derivative line shape overlaps the negative part of the 2,6 proton first derivative leading to cancellation. A similar situation may pertain to the large β-proton $A_{\perp}$ feature 7 which, if it is the same width as the corresponding resonance in the eukaryote spectra, overlaps with the negative part of the 3,5 proton A_z features.

Simulation of EPR Spectra. The hyperfine coupling constants derived from ENDOR spectra should, along with a knowledge of the g factor anisotropy, allow for the simulation of the EPR spectrum of a radical species. We have used a modified version of the simulation program of Brok et al. (1986), kindly provided by C. Hoganson and G. T. Babcock, to support our ENDOR assignments. Simulation of X-band spectra using the hyperfine coupling constants of Table 1 accounts quantitatively for the interspecies variation in EPR line width observed experimentally, Figure 8. The experimental line widths (Hpp) are *P. laminosum* 18.6 G, spinach 19.4, G, and *C. reinhardtii* 20.0 G. However, since X-band spectra of $Y_D^•$ have previously been simulated assuming it to be a quinone (Brok et al., 1985), the ability to simulate the X-band $Y_D^•$ line shape is not strong support for the ENDOR resonance assignments. Therefore we have used the *spinach* $Y_D^•$ data of Table 1 to simulate the following EPR spectra: Q-band (35 GHz, a spectrum of $Y_D^•$ in *Chlorella vulgaris* taken from Brok et al., 1985) Figure 9a,b; spinach S-band (4 GHz) Figure 9c,d; methylene deuterated X-band, Figure 9e,f; and 3,5 deuterated X-band, Figure 9g,h (both deuterated spectra of $Y_D^•$ in *Synechocystis* PCC 6803 from Barry et al. (1990)). The Q-band spectrum shows additional splitting

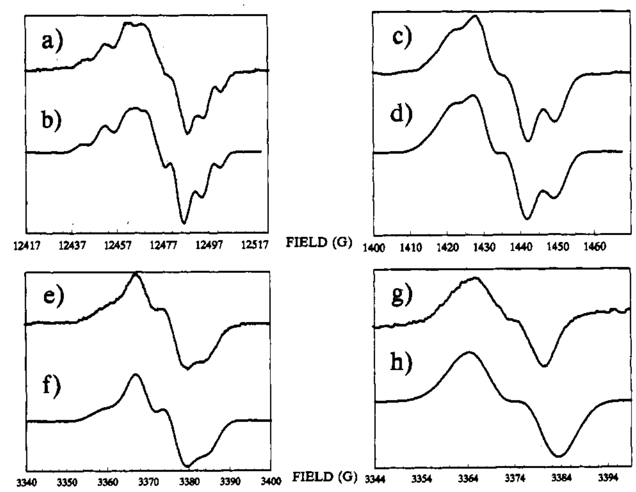

FIGURE 9: EPR spectra (a, c, e, and g) and simulations (b, d, f, and h) of $Y_D^•$. Simulations are all performed with the spinach parameters of Table 1. Actual spectra are *Chlorella vulgaris* at Q-band (a); spinach BBY membranes at S-band (c); *Synechocystis* PS2 with the tyrosine β-methylene protons deuterated, at X-band (e); *Synechocystis* PS2 with the tyrosine 3 and 5 ring protons deuterated, at X-band (g). Simulations were performed and spectra recorded as in Figure 8. Deuteron hyperfine couplings were obtained by multiplying the proton values by 0.154. Other details as given in the text.

due to the increased influence of g factor anisotropy at high fields. This trend is reversed in the S-band spectrum where the g tensor has less of an influence than in X-band. Thus S-band spectra of radicals are more sensitive to changes in hyperfine coupling constants. The only spectrum that is not satisfactorily simulated using the spinach parameters is the 3,5 deuterated X-band spectrum of *Synechocystis*. This is because, as with the three species studied here, the β-methylene proton couplings vary between species. Note that this assertion predicts that the β-methylene deuterated X-band EPR spectrum should be species independent, and therefore the spinach hyperfine couplings should provide for an accurate simulation of the β-methylene deuterated spectrum of *Synechocystis*, as is indeed the case. The g values of Gulin et al. (1992) $g_x = 2.007\ 52$, $g_y = 2.004\ 26$, $g_z = 2.002\ 12$, and Euler angles of ±22° for the 3,5 protons and ±10° for the 2,6 protons were used. Deuteron hyperfine couplings were obtained by multiplying the proton values by 0.154 (Kurreck et al., 1988).

DISCUSSION

EPR spectra of tyrosine radicals in frozen solution exhibit only partially resolved features. The line shapes of these spectra are dominated by two large proton hyperfine couplings (to one β-proton and the protons at the 3 and 5 positions) and are relatively insensitive to the smaller couplings of the system. ENDOR allows these smaller couplings to be resolved, but it has lower sensitivity. However, where the radical of interest interacts magnetically (preferably through a weak dipolar interaction that does not perturb the hyperfine tensors) with another paramagnetic electron spin, conditions may arise in which the radical gives large ENDOR enhancements at low temperatures (liquid helium range, 2–77 K) and high microwave powers (5–20 mW). The use of such temperatures and microwave powers greatly enhances the size of the EPR, and hence the ENDOR, spectrum. We have exploited the relaxation enhancement effect of the OEC in the S_1 state on $Y_D^•$ (Styring & Rutherford, 1988; Evelo et al., 1989) to obtain ENDOR spectra with reasonable signal to noise ratios for samples with concentrations in the range 60–120 μM. The increased resolution of ENDOR has enabled us to demonstrate

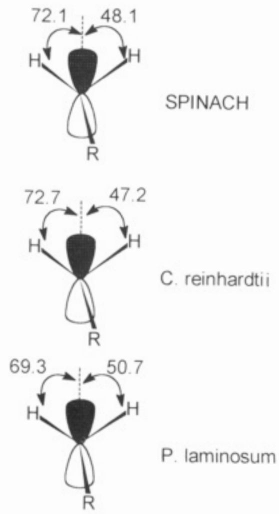

FIGURE 10: Schematic representation of the β-methylene proton dihedral angles, θ, for the three species studied. The view is looking down along the β-carbon to ring carbon 1 bond in Figure 1. The orbital amplitude of the singly occupied molecular orbital (SOMO) at the C1 position is sketched.

interspecies differences in the strong β-methylene proton coupling which are not obvious from the EPR spectra and to measure the hyperfine coupling constants of the weakly coupled β-methylene proton, the 2,6 protons, possibly the α-carbon proton, and at least three weakly coupled matrix protons belonging to the protein. Furthermore inequivalence has been observed between protons 2 and 6 and protons 3 and 5, suggesting that the electron spin density distribution within the aromatic ring is not symmetrical about the carbon 1 (C1)–carbon 4 (C4) axis. This is consistent with studies of in vitro tyrosine neutral radicals in crystals (Box et al., 1974) and in solution at low temperature (Van den Hoek et al., 1970). The latter study suggest that the asymmetry arises from the orientation of the aromatic ring relative to the β-methylene protons. The orientation of the aromatic ring may also be responsible for the different β-methylene proton ENDOR resonance line shapes observed for different species. The increase in the line width of the strongly coupled β-proton resonances from *C. reinhardtii* to spinach to *P. laminosum*, which results in a concomitant decrease in intensity, may result from an increasing small rhombic distortion caused by the change in the orientation of the tyrosine ring relative to the β-methylene protons. No other assignment of the ENDOR spectrum resonances is consistent with the interspecies differences observed here and the published body of knowledge concerning tyrosine radicals.

Having determined the hyperfine coupling constants for both the strongly and weakly coupled β-methylene protons and the ring protons, the electron spin density distribution may be estimated from the McConnell relations (McConnell, 1951; McConnell & Cheshunt, 1958; Derbyshire, 1962; Fessenden & Schuler, 1963):

$$A_{iso} = B\rho \cos^2 \theta \qquad (1)$$

$$A_{iso} = Q\rho \qquad (2)$$

where A_{iso} is the isotropic proton hyperfine coupling constant, ρ is the electron spin density at the attached carbon atom, B and Q are constants relating to β and α protons, respectively, and θ is the dihedral angle defined by the methylene group carbon–proton bond, C1 and the normal to the ring, i.e., the methylene proton conformational angle, Figure 10. This relates the proton hyperfine coupling constants to the electron

Table 2: Calculated Spin Densities and Methylene Angles for $Y_D^{\bullet}$ [a]

	spinach	*C. reinhardtii*	*P. laminosum*
C1	0.4	0.4	0.4
C2 or 6	–0.07	–0.07	–0.07
C2 or 6	–0.08	–0.08	–0.08
C3 or 5	0.26	0.26	0.26
C3 or 5	0.27	0.27	0.27
C4 + O	0.22	0.22	0.22
large coupling θ (deg)	48.1	47.2	50.7
small coupling θ (deg)	72.1	72.7	69.3

[a] Calculations using the McConnell equations (see Discussion for details).

spin density at the attached carbon. Using the values 162 MHz for B (Fessenden & Schuler, 1963; Fasanella & Gordy, 1969) and –69.6 MHz for Q (Bender et al., 1989), we have determined the electron spin densities and β-proton conformational angles (θ) for the $Y_D^{\bullet}$ radical in the three species studied here, Table 2. The determination of the smaller β-proton coupling through ENDOR has enabled us to define θ and the electron spin density at C1 with a far greater precision than is possible using EPR spectroscopy. Proton ENDOR cannot distinguish between electron spin density at ring C4 and the phenoxyl oxygen when the McConnell relations are employed since neither atom has an attached proton. Therefore we have quoted a combined density for C4 and O, Table 2. The electron spin density distribution is essentially identical in all the radicals studied, and the observed differences in their ENDOR spectra, and hence their EPR spectra, arise solely from differences in θ. It is important to note that if θ were fixed at 48.1° and the differences in the large β-coupling were attributed to changes in ρ, then ρC1 spinach would be 0.40, ρC1 *C. reinhardtii* would be 0.42, and ρC1 *P. laminosum* would be 0.36. Since the EPR spectra of the tyrosine radicals are dominated by the large β-proton coupling and are relatively insensitive to the smaller β-proton coupling, it would not be possible to distinguish between these two possible explanations (fixed or different θ) without the small β-proton coupling constants provided by ENDOR spectroscopy.

The only other tyrosine radical for which the electron spin density distribution has been determined is Tyr122 of *E. coli* ribonucleotide reductase (RR) (Bender et al., 1989). This radical has identical electron spin densities to $Y_D^{\bullet}$ at carbons 2, 3, 4, 5, and 6 (although asymmetry about the C1–C4 axis has not been reported for RR Tyr122, perhaps because of the differing value of θ) but has ρC1 of 0.49 and ρC_4/O of 0.13. The crystal structure of RR shows that Tyr122 is not hydrogen bonded at the phenoxyl OH (Nordlund et al., 1990). Predicted structures of PS2 suggest that Y_D is hydrogen bonded through the phenoxyl OH group to D2 His190 or possibly D2 Gln165 (Svensson et al., 1990; Ruffle et al., 1992). This might explain the difference in electron spin density distribution between $Y_D^{\bullet}$ and RR Tyr122.

During the course of these studies we noted the work of Hoganson & Babcock (1992) on $Y_D^{\bullet}$ in *Synechocystis* PCC 6803. Their data were obtained chiefly through the simulation of the EPR spectrum, with only the larger β-proton $A_{\perp}$ and the 3,5 proton A_x hyperfine couplings being obtained using ENDOR. They also obtained ENDOR spectra of $Y_D^{\bullet}$ in spinach which showed both components of the large β-proton coupling. Assuming that all $Y_D^{\bullet}$ EPR spectra were the same, Hoganson and Babcock (1992) attributed the β-proton $A_{\perp}$ resonance in spinach (feature 7, Figure 2) to an artefact arising at a frequency equal to twice the proton Larmor frequency ν_p. This argument follows from studies such as that of

Brustolon and Cassol (Brustolon & Cassol, 1984). However, such artefacts are typically unusually intense with the intensity increasing as the precise value of $2\nu_p$ is approached and decreasing rapidly thereafter. This leads to a distorted line shape. The resonance we observe and assign to the β-proton $A_\perp$ is neither unusually intense nor distorted, being less intense than the 2,6 proton resonances (features 1 and 2 of Figure 2). The value of $2\nu_p$ in our spinach spectra is 28.68 MHz. This point lies between the $A_\perp$ and $A_\parallel$ features in our spinach ENDOR spectrum. The β-proton $A_\parallel$ feature (feature 8, Figure 2) they assign as the A_x component of the 3,5 proton hyperfine coupling. The assignment scheme of Hoganson and Babcock is inconsistent with some of our observations concerning the large β-methylene proton coupling in spinach. Firstly, the two features 7 and 8 move in concert with calcium depletion, Figure 2. The position of the artefact should be a function of $2\nu_p$ which is the same for both spectra. This concerted movement suggests that 7 and 8 are components of the same coupling. Their assignments are also inconsistent with our observation that changes in the positions of these resonances are accompanied by reciprocal changes in another axial system with smaller coupling constants (i.e., the small β-proton coupling). Secondly, in the orientation selection spectra taken at g_x there is a resonance revealed at 27.6 MHz (Figure 4c). This resonance is a negative turning point with two partially resolved components as would be expected for the A_x components of the inequivalent 3 and 5 proton tensors. Feature 8 is also present in this spectrum, Figure 4c. Despite the presence of these two resonances at frequencies close to $2\nu_p$ (28.55 MHz in this species), no equivalent of feature 7 appears. Feature 7 is, however, present in the ENDOR spectrum taken at g_z despite the absence of feature 8 (Figure 7b) and, presumably, the 3,5 protons A_x although the position of the latter lays under feature 7. This behavior is entirely consistent with the assignment of feature 7 as the β-methylene proton $A_\perp$. Of the two turning points present in the spectrum taken at g_x, the resonance at 27.6 MHz fulfills the requirements for the 3,5 proton A_x feature, in terms of line shape and frequency, far more satisfactorily than does feature 8. Note that the low-frequency edge of the 3,5 proton A_x feature is revealed in the spectrum of $Y_D^•$ in calcium-depeleted spinach PS2 (arrowed in Figure 2b), and this edge is not shifted relative to that in Figure 4c. This shows that while features 7 and 8 move on calcium depletion, the underlying A_x component does not. Thirdly, using the hyperfine components of Table 1 we have simulated X-, Q-, and S-band spectra of $Y_D^•$, simulated the previously published β-methylene deuterated spectrum of $Y_D^•$ in *Synechocystis* and shown that the interspecies differences in EPR line width can be accounted for by differences in the β-methylene proton couplings (Figures 8 and 9). Furthermore Hoganson and Babcock (1992) did not provide an alternative assignment for the β-proton ENDOR resonances in spinach since there are no resonances in their spinach ENDOR spectrum (or ours) which correspond to the β-proton resonances of *Synechocystis*. We agree with their large β-proton resonance assignment for *Synechocystis* which is very similar to our assignment for the β-proton resonances of *P. laminosum*. Their electron spin density distribution covers a wide range (ρC1 0.14–0.34, ρC3,5 0.29, ρO 0.45–0.25), as does their range of β-proton conformational angles θ (4–51°), because they lack values for the small coupling constants. However, it is consistent with the data reported here, assuming that their overestimation of ρC3,5 allows ρC1 to approach 0.4. It seems clear that the differences in the interpretation of the spinach ENDOR data between ourselves and Hoganson and Babcock arise from our identification of the interspecies differences in the ring orientation, and hence the EPR and ENDOR spectra, of $Y_D^•$. These differences, while too small to have pronounced affects on the function of $Y_D^•$, do demonstrate the use of ENDOR as a sensitive probe of the electronic structure and orientation of radicals in biological systems. The conservation of the electron spin density distribution in $Y_D^•$ between such diverse organisms as those studied here testifies to the high level of conservation of PS2 structure and function.

The affects of calcium depletion, and other treatments that inhibit oxygen evolution, on $Y_D^•$ are being studied in our laboratories using EPR and ENDOR spectroscopies, and this data will be published separately. ENDOR spectroscopy is also being applied to the tyrosine radical $Y_Z^•$. Ultimately the data presented here will be used to determine the effects of site-directed mutagenesis on the PS2 donor side.

REFERENCES

Babcock, G. T., & Sauer, K. (1973) *Biochim. Biophys. Acta 325*, 483.

Babcock, G. T., Barry, B. A., Debus, R. J., Hoganson, C. W., Atamian, M., McIntosh, L., Sithole, I., & Yocum, C. F. (1989) *Biochemistry 28*, 9557.

Babcock, G. T., El-Deeb, M. K., Sandusky, P. O., Whittaker, M. M., & Whittaker, J. W. (1992) *J. Am. Chem. Soc. 114*, 3727.

Barry, B. A., & Babcock, G. T. (1987) *Proc Natl. Acad. Sci. U.S.A. 84*, 7099.

Barry, B. A., El-Deeb, M. K., Sandusky, P. O., & Babcock, G. T. (1990) *J. Biol. Chem. 265*, 20139.

Bender, C. J., Sahlin, M., Babcock, G. T., Barry, B. A., Chandrashekar, T. K., Salowe, S. P., Stubbe, J., Lindström, B., Petersson, L., Ehrenberg, A., & Sjöberg, B.-M. (1989) *J. Am. Chem. Soc. 111*, 8076.

Berthold, D. A., Babcock, G. T., & Yocum, C. F. (1981) *FEBS Lett. 134*, 231.

Blankenship, R. E., Babcock, G. T., Warden, J. T., & Sauer, K. (1975) *FEBS Lett. 51*, 287.

Boussac, A., Zimmermann, J. L., & Rutherford, A. W. (1989) *Biochemistry 28*, 8984.

Box, H. C., Budzinski, E. E., & Freund, H. G. (1974) *J. Chem. Phys. 61*, 2222.

Brok, M., Ebskamp, F. C. R., & Hoff, A. J. (1985) *Biochim. Biophys. Acta 809*, 421.

Brok, M., Babcock, G. T., DeGroot, A., & Hoff, A. J. (1986) *J. Magn. Reson. 70*, 368.

Brustolon, M., & Cassol, T. (1984) *J. Magn. Reson. 60*, 257.

Chandrashekar, T. K., O'Malley, P. J., Rodriguez, I., & Babcock, G. T. (1986) *Photosyn. Res. 10*, 423.

Commoner, B., Heise, J. J., & Townsend, J. (1956) *Proc. Natl. Acad. Sci. U.S.A. 42*, 718.

Corrie, A. R., Nugent, J. H. A., & Evans, M. C. W. (1991) *Biochim. Biophys. Acta 1057*, 384.

Debus, R. J. (1992) *Biochim. Biophys. Acta 1102*, 269.

Debus, R. J., Barry, B. A., Babcock, G. T., & McIntosh, L. (1988a) *Proc. Natl. Acad. Sci. U.S.A. 85*, 427.

Debus, R. J., Barry, B. A., Sithole, I., Babcock, G. T., & McIntosh, L. (1988b) *Biochemistry 27*, 9071.

DeFilippis, M. R., Murthy, C. P., Faraggi, M., & Klapper, M. H. (1989) *Biochemistry 28*, 4847.

DeFilippis, M. R., Murthy, C. P., Broitman, F., Weintraub, D., Faraggi, M., & Klapper, M. H. (1991) *J. Phys. Chem. 95*, 3416.

DeGray, J. A., Lassman, G., Curtis, J. F., Kennedy, T. A., Marnett, L. J., Eling, T. E., & Mason, R. P. (1992) *J. Biol. Chem. 267*, 23583.

Derbyshire, W. (1962) *Mol. Phys. 5*, 225.

Dixon, W. T., Moghimi, M., & Murphy, D. (1974) *J. Chem. Soc., Faraday Trans. 2/70*, 1713.

Evelo, R. G., Styring, S., Rutherford, A. W., & Hoff, A. J. (1989) *Biochim. Biophys. Acta 973*, 428.

Fasanella, E. L., & Gordy, W. (1969) *Proc. Natl. Acad. Sci. U.S.A. 62*, 229.

Fessenden, R. W., & Schuler, R. H. (1963) *J. Chem. Phys. 39*, 2147.

Ford, R. C., & Evans, M. C. W. (1983) *FEBS Lett. 160*, 159.

Gulin, V. I., Dikanov, S. A., Tsvetkov, Y. D., Evelo, R. G., & Hoff, A. J. (1992) *Pure Appl. Chem. 64*, 903.

Hallahan, B. J., Nugent, J. H. A., Warden, J. T., & Evans, M. C. W. (1992) *Biochemistry 31*, 4562.

Harriman, A. (1987) *J. Phys. Chem. 91*, 6102.

Hoganson, C. W., & Babcock, G. T. (1992) *Biochemistry 31*, 11874.

Janes, S. M., Mu, D., Wemmes, D., Smith, A. J., Kaus, S., Maltby, D., Burlingame, A. L., & Kilman, J. P. (1990) *Science 248*, 981.

Kurreck, H., Kirste, B., & Lubitz, W. (1988) *Electron Nuclear Double Resonance of Radicals in Solution*, 1st ed., VCH Publishers, Inc., New York.

McConnell, H. M. (1956) *J. Chem. Phys. 24*, 764.

McConnell, H. M., & Cheshunt, D. B. (1958) *J. Chem. Phys. 28*, 107.

Metz, J. G., Nixon, P. J., Rögner, M., Brudwig, G. W., & Diner, B. A. (1989) *Biochemistry 28*, 6960.

Nordlund, P., Sjöberg, B.-M., & Eklund, H. (1990) *Nature 345*, 593.

Nugent, J. H. A., Demetriou, C., & Lockett, C. J. (1987) *Biochim. Biophys. Acta 894*, 534.

Nugent, J. H. A., Corrie, A. R., Demetriou, C., Evans, M. C. W., & Lockett, C. J. (1988) *FEBS Lett. 235*, 71.

O'Malley, P. J., & Babcock, G. T. (1984) *J. Chem. Phys. 80*, 3912.

O'Malley, P. J., & Babcock, G. T. (1986) *J. Am. Chem. Soc. 108*, 3995.

O'Malley, P. J., Babcock, G. T., & Prince, R. C. (1984) *Biochim. Biophys. Acta 766*, 283.

Ono, T., & Inoue, Y. (1989) *Biochim. Biophys. Acta 973*, 443.

Rist, G. H., & Hyde, J. S. (1968) *J. Chem. Phys. 49*, 2449.

Ruffle, S. V., Donnelly, D., Blundell, T. L., & Nugent, J. H. A. (1992) *Photosynth. Res. 34*, 287.

Sealy, R. C., Harman, L., West, P. R., & Mason, R. P. (1985) *J. Am. Chem. Soc. 107*, 3401.

Sjöberg, B.-M., & Gräslund, A. (1983) *Adv. Inorg. Biochem. 5*, 87.

Smith, W. L., Eling, T. E., Kulmacz, R. J., Marnett, L. J., & Tsai, A. L. (1992) *Biochemistry 31*, 3.

Styring, S., & Rutherford, A. W. (1987) *Biochemistry 26*, 2401.

Styring, S., & Rutherford, A. W. (1988) *Biochemistry 27*, 4915.

Svensson, B., Vass, I., Cedergren, E., & Styring, S. (1990) *EMBO J. 9*, 2051.

Tomkiewicz, M., McAlpine, R. D., & Cocivera, M. (1972) *Can. J. Chem. 50*, 2849.

Van den Hoek, W. J., Huysmans, W. G. B., & van Gemert, M. J. C. (1970) *J. Magn. Reson. 3*, 137.

Vass, I., & Styring, S. (1991) *Biochemistry 30*, 830.

Vermaas, W. F. J., Rutherford, A. W., & Hansson, Ö (1988) *Proc. Natl. Acad. Sci. U.S.A. 85*, 8477.

Whittaker, M. M., & Whittaker, J. W. (1990) *J. Biol. Chem. 265*, 9610.